The neuroprotective transcription factor ATF5 is decreased and sequestered into polyglutamine inclusions in Huntington's disease

Ivó H. Hernández[1,2,3], Jesús Torres-Peraza[1,2,5], María Santos-Galindo[1,2], Eloísa Ramos-Morón[4], María R. Fernández-Fernández[1,2], María J. Pérez-Álvarez[1,2,3], Antonio Miranda-Vizuete[4] and José J. Lucas[1,2]*

[1] Centro de Biología Molecular Severo Ochoa (CBM"SO") CSIC/UAM, Madrid, Spain.

[2] Instituto de Salud Carlos III, Networking Research Center on Neurodegenerative Diseases (CIBERNED), Spain.

[3] Departamento de Biología, Facultad de Ciencias, Universidad Autónoma de Madrid, Madrid, Spain.

[4] Instituto de Biomedicina de Sevilla, Hospital Universitario Virgen del Rocío/CSIC/Universidad de Sevilla, 41013 Sevilla, Spain

[5] Present Address: Gerència d'Atenció Primària del Servei de Salut de les Illes Balears (IB-SALUT), Palma, Spain

*Corresponding author: José J. Lucas
jjlucas@cbm.uam.es
http://www.cbm.uam.es/lineas/lucasgroup.htm

Abstract

Activating transcription factor-5 (ATF5) is a stress-response transcription factor induced upon different cell stressors like fasting, amino-acid limitation, cadmium or arsenite. ATF5 is also induced, and promotes transcription of anti-apoptotic target genes like *MCL1*, during the unfolded protein response (UPR) triggered by endoplasmic reticulum stress. In the brain, high ATF5 levels are found in gliomas and also in neural progenitor cells, which need to decrease their ATF5 levels for differentiation into mature neurons or glia. This initially led to believe that ATF5 is not expressed in adult neurons. More recently, we reported basal neuronal ATF5 expression in adult mouse brain and its neuroprotective induction during UPR in a mouse model of status epilepticus. Here we aimed to explore whether ATF5 is also expressed by neurons in human brain both in basal conditions and in Huntington's disease (HD), where UPR has been described to be partially impaired due to defective ATF6 processing. Apart from confirming that ATF5 is present in human adult neurons, here we report accumulation of ATF5 within the characteristic polyglutamine-containing neuronal nuclear inclusions in brains of HD patients and mice. This correlates with decreased levels of soluble ATF5 and of its antiapoptotic target MCL1. We then confirmed the deleterious effect of ATF5 deficiency in a *Caenorhabditis elegans* model of polyglutamine-induced toxicity. Finally, ATF5 overexpression attenuated polyglutamine-induced apoptosis in a cell model of HD. These results reflect that decreased ATF5 in HD—probably secondary to sequestration into inclusions—renders neurons more vulnerable to mutant huntingtin-induced apoptosis and that ATF5-increasing interventions might have therapeutic potential for HD.

Keywords: Huntington's disease, ATF5, MCL1, ER stress, UPR, neuroprotection

Introduction

Activating transcription factor-5 (ATF5) [31] is a basic valine/leucine zipper (bZIP) transcription factor that belongs to the ATF/cAMP response-element binding protein (CREB) family [45]. Also known as ATFx or ATF7 [15], ATF5 is a stress-response transcription factor [16] as it is induced by different cell stressors such as fasting [38], amino acid limitation [48], cadmium chloride or sodium arsenite [43]. In line with this, and similar to the related transcription factors ATF4 and ATF6 [17], ATF5 is induced as part of the unfolded protein response (UPR) to cope with the stress induced by the accumulation of unfolded proteins in the endoplasmic reticulum (ER stress) [19, 41, 47, 49]. Such ATF5 induction upon ER stress has been reported to be due to increased transcription [19, 37] and/or to selective translation upon eIF2α-phosphorylation [47, 49]. Essentially, ATF5 plays a pro-survival role as it promotes transcription of antiapoptotic genes such as MCL1 [10, 19, 37]. Accordingly, ATF5 is necessary for survival of many different cell types such as lymphocytes [35] or cardiomyocytes [46]. ATF5 protein expression decreases in cells undergoing apoptosis following growth factor deprivation [35] while its levels are increased and promote apoptotic resistance in a variety of human malignancies, including glioblastoma, breast, pancreatic, lung, and colon cancers [20, 27].

In the brain, highest ATF5 levels are detected in gliomas [1, 27, 37]. In non-pathological brain, high levels are also important for proliferation of neural progenitor cells and a significant decrease in their ATF5 levels is required for their differentiation into mature neurons or glial cells [2, 3, 24]. This led to the notion of ATF5 not being expressed in adult neurons [14]. However, we have demonstrated that mouse adult neurons maintain a steady state level of ATF5 expression which increases upon UPR-triggering stimuli such as tunicamycin or the status epilepticus caused by intra-amygdala injection of kainic acid [41]. This neuronal ATF5 induction is believed to be neuroprotective as ATF5 overexpression attenuates ER stress-induced apoptosis in neurons [41].

Huntington's disease (HD) is the most common genetically determined neurodegenerative disease and belongs to the group of neurological disorders caused by expanded CAG triplet repeats encoding self-aggregating poly-glutamine (polyQ) tracts in their respective proteins [33]. HD is characterized by marked atrophy in the caudate and putamen and to a lesser extent in the cortex and by the presence of polyQ-containing inclusions bodies (IBs). ER stress activation and/or impairment is a common feature of most neurodegenerative diseases including HD [18] and we and others have previously reported impaired UPR execution in HD due to diminished processing of ATF6 [11, 30]. In view of the putative neuroprotective role of ATF5 upon ER stress induction and its constitutive expression in mouse adult neurons [41], we decided to explore the status of ATF5 in HD mouse models and human tissue.

Materials and Methods

Human brain tissue samples

Brain specimens used in this study from frontal cortex and striatum of HD patients and controls were provided by Institute of Neuropathology (HUB-ICO-IDIBELL) Brain Bank (Hospitalet de Llobregat, Spain), the Neurological Tissue Bank of the IDIBAPS Biobank (Barcelona, Spain), the Banco de Tejidos Fundación Cien (BT-CIEN, Madrid, Spain), and the Netherlands Brain Bank (Amsterdam, The Netherlands). Written informed consent for brain removal after death for diagnostic and research purposes was obtained from brain donors and/or next of kin. Procedures, information and consent forms have been approved by the Bioethics Subcommittee of Consejo Superior de Investigaciones Científicas (CSIC, Madrid, Spain). When available, the neuropathological examination of HD cases to assign HD grade from 0–1 to 4 following Vonsattel's criteria, and the number of CAG repeats is shown in Supplementary Table 1. The postmortem interval in tissue processing is also indicated in Supplementary Table 1.

Mice

R6/1 transgenic mice for the human exon-1-HTT gene [23] in B6CBAF1 background were housed at the Centro de Biología Molecular "Severo Ochoa" animal facility. Mice were housed four per cage with food and water available ad libitum and maintained in a temperature-controlled environment on a 12/12 h light–dark cycle with light onset at 0800 hours. Animal housing and maintenance protocols followed the guidelines of Council of Europe Convention ETS123. Animal experiments were performed under protocols (PROEX293/15) approved by the Centro de Biología Molecular Severo Ochoa Institutional Animal Care and Utilization Committee (Comité de Ética de Experimentación Animal del CBM, CEEA-CBM), Madrid, Spain.

Caenorhabditis elegans

The standard methods used for culturing and maintenance of *C. elegans* were as previously described [40]. The strains used in this work are: N2, *wild type DR subclone of CB original (Tc1 pattern I)*, LD1325, *atf-5(tm4397) X [12]*, VZ531 = *vzEx173 [Punc-54::Q40::yfp]*, VZ533 = *vzEx175 [Punc-54::Q40::yfp]*, VZ534 = *atf-5(tm4397) X*; *vzEx173 [Punc-54::Q40::yfp]* and VZ535 = *atf-5(tm4397) X*; *vzEx175 [Punc-54::Q40::yfp]*. All experiments were performed at 20 °C unless otherwise noted. All VZ strains are 6× backcrossed and LD1325 is 7× backcrossed with *N2 wild type*.

Cell culture and transfection

Neuro-2a neuroblastoma cells were cultured in 10% FBS (GIBCO) supplemented DMEM at 37 °C in a 5% CO_2 atmosphere. The day before transfection 3 × 105 cells per condition were placed in a six well plate (Falcon), with or without glass coverslips, and allowed to attach to the plate. N2a cells were transfected (Lipofectamine 2000, Thermo Fisher) with the following construct combinations: PolyQ16 and pcDNA3; PolyQ94 and pcDNA3; PolyQ94 and pcDNA3-MYC-mATF5; PolyQ94 and p3XFlag-CMV10-Flag-mMcl-1. PolyQ16, PolyQ94, pcDNA3-MYC-mATF5 and p3XFlag-CMV10-Flag-mMcl-1 plasmids were previously described [25, 39, 41]. After transfection for 48 h, the transfected cells were used for subsequent assays.

Tissue Preparation

For human samples, formalin-fixed (4%, 24 h), paraffin-embedded tissue from cortex and striatum were used. Sections (5-µm thick) were mounted on superfrost-plus tissue slides (Menzel-Gläser) and deparaffinized. Peroxidase activity was quenched with 0.3% H_2O_2 in methanol for 30 min, followed by antigen retrieval with 10 mM pH 6.0 citrate buffer heated by microwave for 15 min.

Mice euthanasia was performed using CO_2. Brains were immediately removed and dissected on an ice-cold plate and left hemispheres, processed for histology, placed in 4% paraformaldehyde in Sorensen's phosphate buffer overnight and then immersed in 30% sucrose in PBS for 72 h. Once cryoprotected, samples were included in optimum cutting temperature (OCT) compound (Tissue-Tek, Sakura Finetek Europe, ref. 4583), frozen and stored at −80 °C before use. 30 µm sagittal sections were cut on a cryostat (Thermo Scientific), collected and stored free floating in glycol containing buffer (30% glycerol, 30% ethylene glycol in 0.02 M phosphate buffer) at −20 °C.

Immunohistochemistry and Immunofluorescence

For immunohistochemical staining, sections were first washed with PBS and immersed in 0.3% H_2O_2 in PBS for 45 min to quench endogenous peroxidase activity. Sections were then immersed for 1 h in blocking solution (PBS containing 0.5% Fetal Bovine Serum, 0.3% Triton X-100 and 1% BSA) and incubated overnight at 4 °C with rabbit anti-ATF5 (1:1000, AVIVA, ARP30970) diluted in blocking solution. After washing, brain sections were incubated first with biotinylated goat anti-rabbit secondary antibody and then with avidin–biotin complex using the Elite Vectastain kit (Vector Laboratories, PK-6101-2). Chromogen reactions were performed with diaminobenzidine (SIGMA-FAST DAB, Sigma, D4293) for 10 min. Mouse sections were mounted on glass slides and coverslipped with Mowiol (Calbiochem, Cat. 475904) while human sections where first dehydrated and then mounted with DePex (SERVA). Images were captured using an Olympus BX41 microscope with an Olympus camera DP-70 (Olympus Denmark A/S).

For immunofluorescence, brain sections and N2a coverslips were pretreated with 0.1% Triton X-100 for 30 min, 1 M glycine for 15 min and blocking solution (1% BSA, 0.3% FBS and 0.1% Triton X-100) for 1 h. Sections were then incubated overnight at 4 °C with rabbit anti-ATF5 (1:1000, AVIVA, ARP30970) and goat anti-huntingtin (1:200, N-18 Santa Cruz, sc-8767) in blocking solution. The

following day, sections were washed in PBS and incubated with secondary antibodies for 1 h: anti-goat Alexa 555 (1:500, ThermoFisher, A-21432) and anti-rabbit Alexa 488 (1:500, ThermoFisher, A-21206). After washing, nuclei were counterstained with DAPI (1:5000, Calbiochem, 28718-90-3) for 3 min. Finally, sections were mounted on glass slides, coverslipped with Mowiol (Calbiochem, 475904) and maintained at 4 °C. N2a coverslips were co-incubated with rabbit anti-cleaved caspase 3 (1:100, Cell Signaling, 9579) and goat anti-ATF5 (1:1000, Santa Cruz, sc-377168) for 1 h at room temperature. Coverslips were then washed with PBS and co-incubated with anti-goat Alexa 555 (A-21432) and anti-rabbit Alexa 647 (A-31573) for 1 h. Nuclei were counterstained as with tissue sections. Coverslips were mounted in FluorSave (Calbiochem, Merck KGaA). Images were acquired with a laser confocal LSM710 system coupled to the invert Axioobserver microscope with a 63×, 1.4 numerical aperture oil-immersion objective using the Zen2010B sp1 software (Carl Zeiss). Sequential optic sections (1 µm) were acquired in z stacks. Images were processed using ImageJ 1.45s.

Western Blot

Samples from human brain were stored at −80 °C and ground with a mortar in a frozen environment with liquid nitrogen to prevent thawing of the samples, resulting in tissue powder. Mouse brains were quickly dissected on an ice-cold plate and the different structures stored at −80 °C. Human and mouse protein extracts were prepared by homogenizing brain structures in ice-cold extraction buffer [20 mM HEPES pH 7.4, 100 mM NaCl, 20 mM NaF, 1% Triton X-100, 1 mM sodium orthovanadate, 1 µM okadaic acid, 5 mM sodium pyrophosphate, 30 mM β-glycerophosphate, 5 mM EDTA, protease inhibitors (Complete, Roche, Cat. No 11697498001)]. Homogenates were centrifuged at 15,000 rpm for 15 min at 4 °C. The resulting supernatant was collected, and protein content determined by Quick Start Bradford Protein Assay (Bio-Rad, 500-0203). 20 µg of total protein were electrophoresed on 10% SDS–polyacrylamide gel,

transferred to a nitrocellulose blotting membrane (Amersham Protran 0.45 µm, GE Healthcare Life Sciences, 10600002) and blocked in TBS-T (150 mM NaCl, 20 mM Tris–HCl, pH 7.5, 0.1% Tween 20) supplemented with 5% non-fat dry milk. Membranes were incubated overnight at 4 °C with either rabbit anti-ATF5 (1:1000, AVIVA, ARP30970), rabbit anti-MCL1 (1:1000, Santa Cruz, sc-819), mouse anti-TUBB3 (1:5000; Novus Biologicals, NB120-11314) or mouse anti-β-ACTIN (1:50,000, SIGMA, A2066) in TBS-T supplemented with 5% non-fat dry milk, washed with TBS-T and next incubated with HRP-conjugated anti-rabbit IgG (1:2000, DAKO, P0448) and developed using the ECL detection kit (PerkinElmer, NEL105001EA).

Data analysis.

Statistical analysis was performed with SPSS 21.0 (SPSS® Statistic IBM®). Data are represented as Mean ± SEM (standard error of the mean). The normality of the data was analyzed by Shapiro–Wilk or Kolmogorov–Smirnov tests. For two-group comparison, two-tailed *t* Student's test was performed. For multiple comparisons, data were analyzed by one way-ANOVA test followed by an LSD or a Games–Howell post hoc test. A critical value for significance of $p < 0.05$ was used throughout the study.

Results

ATF5 is sequestered into neuronal polyQ inclusions in HD mouse model and human tissue

We first performed ATF5 immunohistochemistry (IHC) on brain sections from an HD mouse model and matching wild type mice. More precisely, we analyzed the widely used R6/1 transgenic mouse model of expanded CAG/polyQ disease that ubiquitously expresses N-terminal huntingtin (*HTT*) with 115 CAG repeats [23]. Cortex and striatum were analyzed as these are the most affected brain regions in HD and the most salient feature was the bold accumulation of ATF5 immunoreactivity in neuronal nuclear inclusion bodies (IBs) in both brain regions of R6/1 but not in wild type mice (Fig. 1a). Interestingly, this accumulation of ATF5 in IBs of R6/1 mice is an early event as it can be observed from an early-symptomatic age (3.5 months). We then performed ATF5 IHC on human HD and control tissue which for the first time demonstrated expression of ATF5 in human adult neurons (Fig. 1b) in line with our previous observations in mouse tissue [41]. Furthermore, ATF5 immunostaining also confirmed accumulation of ATF5 into neuronal nuclear aggregates that resemble the characteristic polyQ IBs in HD brains (Fig. 1b). Apart from nuclear inclusions, HD patients also show inclusions in the soma and neurites and, interestingly, ATF5 can also be found in cytoplasmic inclusions in the soma, in neuritic inclusions, and in neuropil inclusions (Fig. 1c).

To confirm that ATF5 is in fact being sequestered into the polyQ-containing neuronal nuclear IBs, we performed double immunofluorescence with antibodies against ATF5 and N-terminal mutant HTT (mHTT). As shown in Fig. 2, ATF5-positive nuclear inclusions colocalized with mHTT nuclear inclusions both in R6/1 mouse tissue (Fig. 2a) (Pearson correlation coefficient = 0.7) and in human HD tissue (Fig. 2b) (Pearson correlation coefficient = 0.78).

Decreased ATF5 levels in striatum and cortex of HD mouse model and human tissue

We then performed Western blot analysis to test whether accumulation of ATF5 within mHTT IBs correlates with decreased levels of soluble monomeric ATF5. We decided to analyze R6/1 mice at the age of 3.5 months when they are pre- or early-symptomatic with very little striatal atrophy and neuronal loss [22] and we observed a 40.5% reduction of ATF5 levels in the striatum respect to wild type ($p = 0.0003$) (Fig. 3a). In cortex of R6/1 mice, we also observed a significant although less pronounced decrease in the levels of ATF5 (18.9% decrease, $p < 0.05$) (Fig. 3a). In HD patient postmortem brains, we also observed decreased ATF5 levels both in cortex and caudate/putamen, with respect to samples from control subjects (Fig. 3b). In this case, the decrease was more pronounced and more significant in cortex (78.5% decrease, $p = 0.0001$) than in striatal nuclei (24.7% decrease, $p = 0.006$). Since HD patient postmortem striatum do show significant neuronal loss, we decided to normalize the levels of ATF5 to the level of the neuronal marker beta-III tubulin (TUBB3) [4]. When applying this correction for the effect of neuronal loss, the ATF5 decrease is still significant in cortex (66.2% decrease, $p = 0.04$) while only a tendency in striatum. This suggests that, at least in part, neuronal loss contributes to the decreased striatal ATF5 levels observed respect to total protein content.

Decreased levels of the antiapoptotic ATF5 target MCL1 in striatum and cortex of HD mouse model and human tissue

We then wondered whether decreased levels of ATF5 would correlate with decreased levels of its target MCL1 which has been proposed to play an important role in the antiapoptotic actions of ATF5 [19, 37]. For this, we performed Western blot analysis of MCL1 on HD mouse model and human tissue samples. As expected, a marked decrease in MCL1 levels was observed in striatum (53.1% decrease, $p < 0.0001$) and in cortex (47.4% decrease, $p = 0.016$) of 3.5 month old R6/1 mice with

respect to age-matched wild type controls (Fig. 4a). Similar results of decreased MCL1 levels were also observed in striatum (77.7% decrease, $p < 0.0001$) and cortex (55% decrease, $p = 0.002$) of HD patients respect to control subjects (Fig. 4b).

Deleterious effect of ATF5 deficiency in a *C. elegans* model of polyQ toxicity

To gain insight into the potential deleterious effect of decreased ATF5 in an in vivo context of polyQ-induced toxicity, we moved to the nematode model *C. elegans*. Specifically, we used a *C. elegans* strain that carries the transgene *vzEx173 [Punc-54::Q40::yfp]* resulting in the expression of a fusion protein Q40::YFP in worm muscle cells (*Q40::yfp* expression is controlled by the *unc-54* myosin heavy chain gene promoter), causing an age-dependent aggregation phenotype whose readout is a progressive motility deficit [29]. Thus, we generated worms expressing the *vzEx173 [Punc-54::Q40::yfp]* transgene in an *atf-5(tm4397)* null mutant background and found that lack of *atf-5* causes an increase in the number of Q40::YFP aggregates (Fig. 5a, b). Interestingly, while *atf-5* deficiency does not provoke any motility defect in otherwise wild type worms, we found a marked decrease in motility when the *atf-5* mutation was introduced in the Q40::YFP expressing background (Fig. 5c). Similar results were obtained when using another independent transgene *vzEx175 [Punc-54::Q40::yfp]* (data not shown). Together, these results indicate that decreased ATF5 levels exacerbate polyQ-toxicity in vivo.

ATF5 protects from polyglutamine-induced apoptosis in a cell model of HD

The decreased levels of ATF5 and of its antiapoptotic target MCL1 in the brain of the R6/1 HD mouse model and patients, together with the deleterious effect of *atf-5* deficiency in polyQ-expressing *C. elegans* strains, suggest that increasing ATF5 levels might be beneficial through attenuation of polyQ-induced apoptosis. To test this, we performed experiments on N2a neuroblastoma cells.

First, we verified that transfection of an ATF5 expression vector increased both ATF5 and MCL1 protein levels (Fig. 6a). Then, we verified that transfection of mHTT fused to CFP (PolyQ94), but not wild type N-terminal HTT fused to CFP (PolyQ16), resulted in IB formation (Fig. 6b, c) and in polyQ-induced apoptosis as evidenced by cleaved caspase-3 immunofluorescence or by DAPI nuclear counterstaining (Fig. 6c, d). Co-transfection of ATF5 with PolyQ94 resulted in increased diffuse ATF5 levels despite accumulation of ATF5 within polyQ inclusions (Fig. 6b). Besides, we observed that the incidence of apoptosis in PolyQ94 + ATF5 cells was much lower than in PolyQ94 cells and comparable to that in PolyQ16 cells (Fig. 6c, d), thus demonstrating that ATF5 overexpression is protective against polyQ-induced apoptosis. We also assayed the effect of the sole overexpression of MCL1 on polyQ94-induced apoptosis. As shown in Fig. 6e–g, MCL1 overexpression by itself also significantly reduced the rate of apoptosis induced by PolyQ94 to levels comparable to those in PolyQ16 cells. This confirms that the increased MCL1 levels induced by ATF5 overexpression contribute to the neuroprotective effect of ATF5.

Discussion

Here we first report accumulation of ATF5 within the characteristic neuronal polyQ-containing IBs in the brain of HD mice starting at early-symptomatic ages and also in postmortem human HD brain tissue. This sequestration of ATF5 into IBs correlates with a decrease in the level of soluble ATF5 in both mouse and human HD tissue and with decreased levels of the antiapoptotic ATF5 target MCL1. Here we also analyze a nematode model of polyQ-induced toxicity which confirmed the deleterious effect of ATF5 deficiency. Finally, we show that ATF5 overexpression attenuates polyQ-induced apoptosis in a neuroblastoma cell model of HD. Together these results indicate that decreased levels of ATF5 in HD brain—probably secondary to its sequestration into polyQ IBs—render neurons more vulnerable to mutant huntingtin-induced apoptosis.

We have previously shown that, contrary to the previous notion of adult neurons not expressing ATF5 [14], adult mice do show steady state levels of ATF5 expression in neurons [41]. Now, by showing ATF5 accumulation into neuronal IBs in human HD brain together with the diffuse ATF5 immunostaining in neurons of control and HD brains, we here extend to humans the previous observation of ATF5 being expressed by adult neurons.

There are different possible mechanisms by which ATF5 could accumulate into polyQ-containing IBs in brains of HD patients and mouse models. For instance, it is known that many transcription factors bind expanded polyQ stretches and are often found sequestered into IBs [32]. These include CREB-binding protein (CBP), SP1, TBP, p53 [32] and many others such as the bZIP transcription factor C/EBPα [8]. Since bZIP containing transcription factors have the ability to form heterodimers [15], it is possible that ATF5 could reach the polyQ IBs through indirect interaction with any of the transcription factors previously reported to accumulate into polyQ IBs. Alternatively, it is known

that ATF5 has by itself propensity to aggregate in vitro [5, 6]. It is therefore possible that ATF5 could self-aggregate in vivo in pathophysiological conditions such as HD in which proteostasis and quality control mechanisms are compromised [7, 34, 44]. Such ATF5 microaggregates could then coalesce into mature IBs [21] such as those containing other polyQ-driven aggregates.

We have mentioned that the decrease in soluble ATF5 might be secondary to its sequestration into IBs. An indicator in favor of this possibility is that the decrease in ATF5 protein levels in brain of HD mice and patients takes place without a matching decrease in its mRNA levels (data not shown). Therefore, the decrease in protein levels will most likely be secondary to decreased translation or to diminished half-life of the soluble protein, for instance because it gets aggregated. In fact, there are multiple examples of proteins whose sequestration into polyQ-IBs correlates with decreased soluble levels and loss of function [13, 26].

Regardless of the mechanism by which it takes place, we here provide evidence of decreased ATF5 being deleterious, probably, because it contributes to a deficient execution of the UPR in HD in line with the previously reported deficient processing of ATF6 in HD patients and mouse models [11, 30]. Such deficient UPR execution will have proapoptotic effect as we show here that it is paralleled by a decrease in the levels of MCL1, a well-established target of ATF5 with antiapoptotic actions. Therefore, in line with the here shown neuroprotective effect of ATF5 overexpression in a cell model of HD, any pharmacological intervention able to increase ATF5 levels in HD might be of therapeutic value. In this regard, salubrinal, guanabenz and sephin1 are small drugs that prolong eIF2α phosphorylation by inhibiting PPP1R15A (GADD34) and therefore modulate the UPR [9, 42]. Accordingly, salubrinal increases ATF5 levels in primary neuronal cultures [41] and it has been shown to attenuate cell death induced by the ER stress inducer tunicamycin [41] and also by N-terminal

mutant HTT [36]. This suggests that salubrinal or any other of the PPP1R15A inhibitors might be beneficial in HD. However, there might also be unwanted effects as in vivo administration of salubrinal has been reported to increase toxicity in a mouse model of prion-induced neurodegeneration [28].

In summary, here we report that reduced levels of ATF5

in brain of HD patients, probably due to its sequestration into the characteristic PolyQ containing neuronal IBs, correlates with decreased levels of the antiapoptotic protein MCL1, a transcriptional target of ATF5. We also provide evidence of decreased ATF5 being deleterious by rendering neurons more vulnerable to polyQ-induced apoptosis, thus suggesting that ATF5-increasing pharmacological interventions might open future therapeutic opportunities for HD.

Acknowledgements

This work was supported by CiberNed-ISCIII collaborative Grants PI2013/09-2 and PI2015-2/06-3 and by grants from Spanish Ministry of Economy and Competitiveness (MINECO): SAF2009-08233 and SAF2015-65371-R to JJL, by Fundación BBVA and by Fundación Ramón Areces. Human tissue was obtained from Institute of Neuropathology (HUB-ICO-IDIBELL) Brain Bank, the Neurological Tissue Bank of the IDIBAPS Biobank, the Banco de Tejidos Fundación CIEN, and the Netherlands Brain Bank. We thank Prof. Keith Blackwell for providing the LD1325 *C. elegans* strain. We also thank excellent technical assistance by Miriam Lucas and by the following core facilities: CBMSO-Genomics and Massive Sequencing and CBMSO-Animal Facility.

Compliance with ethical standards

Conflict of interest

The authors declare that they have no conflict of interest.

REFERENCES:

1. Angelastro JM, Canoll PD, Kuo J, Weicker M, Costa A, Bruce JN, Greene LA (2006) Selective destruction of glioblastoma cells by interference with the activity or expression of ATF5. Oncogene 25:907–916
2. Angelastro JM, Ignatova TN, Kukekov VG, Steindler DA, Stengren GB, Mendelsohn C, Greene LA (2003) Regulated expression of ATF5 is required for the progression of neural progenitor cells to neurons. J Neurosci 23:4590–4600
3. Angelastro JM, Mason JL, Ignatova TN, Kukekov VG, Stengren GB, Goldman JE, Greene LA (2005) Downregulation of activating transcription factor 5 is required for differentiation of neural progenitor cells into astrocytes. J Neurosci 25:3889–3899
4. Caccamo DV, Herman MM, Frankfurter A, Katsetos CD, Collins VP, Rubinstein LJ (1989) An immunohistochemical study of neuropeptides and neuronal cytoskeletal proteins in the neuroepithelial component of a spontaneous murine ovarian teratoma. Primitive neuroepithelium displays immunoreactivity for neuropeptides and neuron-associated beta-tubulin isotype. Am J Pathol 135:801–813
5. Ciaccio NA, Laurence JS (2009) Effects of disulfide bond formation and protein helicity on the aggregation of activating transcription factor 5. Mol Pharm 6:1205–1215
6. Ciaccio NA, Reynolds TS, Middaugh CR, Laurence JS (2012) Influence of the valine zipper region on the structure and aggregation of the basic leucine zipper (bZIP) domain of activating transcription factor 5 (ATF5). Mol Pharm 9:3190–3199
7. Cortes CJ, La Spada AR (2014) The many faces of autophagy dysfunction in Huntington's disease: from mechanism to therapy. Drug Discov Today 19:963–971
8. Chiang MC, Chen HM, Lee YH, Chang HH, Wu YC, Soong BW, Chen CM, Wu YR, Liu CS, Niu DM et al (2007) Dysregulation of C/EBPalpha by mutant huntingtin causes the urea cycle deficiency in Huntington's disease. Hum Mol Genet 16:483–498
9. Das I, Krzyzosiak A, Schneider K, Wrabetz L, D'Antonio M, Barry N, Sigurdardottir A, Bertolotti A (2015) Preventing proteostasis diseases by selective inhibition of a phosphatase regulatory subunit. Science (New York, NY) 348:239–242
10. Dluzen D, Li G, Tacelosky D, Moreau M, Liu DX (2011) BCL-2 is a downstream target of ATF5 that mediates the prosurvival function of ATF5 in a cell type-dependent manner. J Biol Chem 286:7705–7713
11. Fernandez-Fernandez MR, Ferrer I, Lucas JJ (2011) Impaired ATF6alpha processing, decreased Rheb and neuronal cell cycle re-entry in Huntington's disease. Neurobiol Dis 41:23–32
12. Ferraz RC, Camara H, De-Souza EA, Pinto S, Pinca AP, Silva RC, Sato VN, Castilho BA, Mori MA (2016) IMPACT is a GCN2 inhibitor that limits lifespan in Caenorhabditis elegans. BMC Biol 14:87. doi:10.1186/s12915-016-0301-2
13. Fujita K, Nakamura Y, Oka T, Ito H, Tamura T, Tagawa K, Sasabe T, Katsuta A, Motoki K, Shiwaku H et al (2013) A functional deficiency of TERA/VCP/p97 contributes to impaired DNA repair in multiple polyglutamine diseases. Nat Commun 4:1816
14. Greene LA, Lee HY, Angelastro JM (2009) The transcription factor ATF5: role in neurodevelopment and neural tumors. J Neurochem 108:11–22

15. Hai T, Hartman MG (2001) The molecular biology and nomenclature of the activating transcription factor/cAMP responsive element binding family of transcription factors: activating transcription factor proteins and homeostasis. Gene 273:1–11
16. Hatano M, Umemura M, Kimura N, Yamazaki T, Takeda H, Nakano H, Takahashi S, Takahashi Y (2013) The 5'-untranslated region regulates ATF5 mRNA stability via nonsense-mediated mRNA decay in response to environmental stress. FEBS J 280:4693–4707
17. Hetz C (2012) The unfolded protein response: controlling cell fate decisions under ER stress and beyond. Nat Rev Mol Cell Biol 13:89–102
18. Hetz C, Mollereau B (2014) Disturbance of endoplasmic reticulum proteostasis in neurodegenerative diseases. Nat Rev Neurosci 15:233–249
19. Izumi S, Saito A, Kanemoto S, Kawasaki N, Asada R, Iwamoto H, Oki M, Miyagi H, Ochi M, Imaizumi K (2012) The endoplasmic reticulum stress transducer BBF2H7 suppresses apoptosis by activating the ATF5-MCL1 pathway in growth plate cartilage. J Biol Chem 287:36190–36200
20. Karpel-Massler G, Horst BA, Shu C, Chau L, Tsujiuchi T, Bruce JN, Canoll P, Greene LA, Angelastro JM, Siegelin MD (2016) A synthetic cell-penetrating dominant-negative ATF5 peptide exerts anticancer activity against a broad spectrum of treatment-resistant cancers. Clin Cancer Res 22:4698–4711
21. Kopito RR (2000) Aggresomes, inclusion bodies and protein aggregation. Trends Cell Biol 10:524–530
22. Li JY, Popovic N, Brundin P (2005) The use of the R6 transgenic mouse models of Huntington's disease in attempts to develop novel therapeutic strategies. NeuroRx J Am Soc Exp NeuroTher 2:447–464. doi:10.1602/neurorx.2.3.447
23. Mangiarini L, Sathasivam K, Seller M, Cozens B, Harper A, Hetherington C, Lawton M, Trottier Y, Lehrach H, Davies SW et al (1996) Exon 1 of the HD gene with an expanded CAG repeat is sufficient to cause a progressive neurological phenotype in transgenic mice. Cell 87:493–506
24. Mason JL, Angelastro JM, Ignatova TN, Kukekov VG, Lin G, Greene LA, Goldman JE (2005) ATF5 regulates the proliferation and differentiation of oligodendrocytes. Mol Cell Neurosci 29:372–380
25. Maynard CJ, Bottcher C, Ortega Z, Smith R, Florea BI, Diaz-Hernandez M, Brundin P, Overkleeft HS, Li JY, Lucas JJ et al (2009) Accumulation of ubiquitin conjugates in a polyglutamine disease model occurs without global ubiquitin/proteasome system impairment. Proc Natl Acad Sci USA 106:13986–13991
26. McCampbell A, Taylor JP, Taye AA, Robitschek J, Li M, Walcott J, Merry D, Chai Y, Paulson H, Sobue G et al (2000) CREB-binding protein sequestration by expanded polyglutamine. Hum Mol Genet 9:2197–2202
27. Monaco SE, Angelastro JM, Szabolcs M, Greene LA (2007) The transcription factor ATF5 is widely expressed in carcinomas, and interference with its function selectively kills neoplastic, but not nontransformed, breast cell lines. Int J Cancer 120:1883–1890
28. Moreno JA, Radford H, Peretti D, Steinert JR, Verity N, Martin MG, Halliday M, Morgan J, Dinsdale D, Ortori CA et al (2012) Sustained translational repression by eIF2alpha-P mediates prion neurodegeneration. Nature 485:507–511

29. Morley JF, Brignull HR, Weyers JJ, Morimoto RI (2002) The threshold for polyglutamine-expansion protein aggregation and cellular toxicity is dynamic and influenced by aging in Caenorhabditis elegans. Proc Natl Acad Sci USA 99:10417–10422
30. Naranjo JR, Zhang H, Villar D, Gonzalez P, Dopazo XM, Moron-Oset J, Higueras E, Oliveros JC, Arrabal MD, Prieto A et al (2016) Activating transcription factor 6 derepression mediates neuroprotection in Huntington disease. J Clin Investig 126:627–638
31. Nishizawa M, Nagata S (1992) cDNA clones encoding leucine-zipper proteins which interact with G-CSF gene promoter element 1-binding protein. FEBS Lett 299:36–38
32. Okazawa H (2003) Polyglutamine diseases: a transcription disorder? Cell Mol Life Sci 60:1427–1439
33. Orr HT, Zoghbi HY (2007) Trinucleotide repeat disorders. Annu Rev Neurosci 30:575–621
34. Ortega Z, Diaz-Hernandez M, Lucas JJ (2007) Is the ubiquitin-proteasome system impaired in Huntington's disease? Cell Mol Life Sci 64:2245–2257
35. Persengiev SP, Devireddy LR, Green MR (2002) Inhibition of apoptosis by ATFx: a novel role for a member of the ATF/CREB family of mammalian bZIP transcription factors. Genes Dev 16:1806–1814
36. Reijonen S, Putkonen N, Norremolle A, Lindholm D, Korhonen L (2008) Inhibition of endoplasmic reticulum stress counteracts neuronal cell death and protein aggregation caused by N-terminal mutant huntingtin proteins. Exp Cell Res 314:950–960
37. Sheng Z, Li L, Zhu LJ, Smith TW, Demers A, Ross AH, Moser RP, Green MR (2010) A genome-wide RNA interference screen reveals an essential CREB3L2-ATF5-MCL1 survival pathway in malignant glioma with therapeutic implications. Nat Med 16:671–677
38. Shimizu YI, Morita M, Ohmi A, Aoyagi S, Ebihara H, Tonaki D, Horino Y, Iijima M, Hirose H, Takahashi S et al (2009) Fasting induced up-regulation of activating transcription factor 5 in mouse liver. Life Sci 84:894–902
39. Stewart DP, Koss B, Bathina M, Perciavalle RM, Bisanz K, Opferman JT (2010) Ubiquitin-independent degradation of antiapoptotic MCL-1. Mol Cell Biol 30:3099–3110. doi:10.1128/ MCB.01266-09
40. Stiernagle T (2006) Maintenance of C. elegans. In: WormBook, The C. elegans Research Community, eds., pp 1–11. doi:10.1895/ wormbook.1.101.1. http://www.wormbook.org
41. Torres-Peraza JF, Engel T, Martin-Ibanez R, Sanz-Rodriguez A, Fernandez-Fernandez MR, Esgleas M, Canals JM, Henshall DC, Lucas JJ (2013) Protective neuronal induction of ATF5 in endoplasmic reticulum stress induced by status epilepticus. Brain 136:1161–1176
42. Tsaytler P, Harding HP, Ron D, Bertolotti A (2011) Selective inhibition of a regulatory subunit of protein phosphatase 1 restores proteostasis. Science (New York, NY) 332:91–94
43. Uekusa H, Namimatsu M, Hiwatashi Y, Akimoto T, Nishida T, Takahashi S, Takahashi Y (2009) Cadmium interferes with the degradation of ATF5 via a post-ubiquitination step of the proteasome degradation pathway. Biochem Biophys Res Commun 380:673–678
44. Vidal R, Caballero B, Couve A, Hetz C (2011) Converging pathways in the occurrence of endoplasmic reticulum (ER) stress in Huntington's disease. Curr Mol Med 11:1–12
45. Vinson C, Myakishev M, Acharya A, Mir AA, Moll JR, Bonovich M (2002) Classification of human B-ZIP proteins based on dimerization properties. Mol Cell Biol 22:6321–6335

46. Wang H, Lin G, Zhang Z (2007) ATF5 promotes cell survival through transcriptional activation of Hsp27 in H9c2 cells. Cell Biol Int 31:1309–1315
47. Watatani Y, Ichikawa K, Nakanishi N, Fujimoto M, Takeda H, Kimura N, Hirose H, Takahashi S, Takahashi Y (2008) Stress-induced translation of ATF5 mRNA is regulated by the 5'-untranslated region. J Biol Chem 283:2543–2553
48. Watatani Y, Kimura N, Shimizu YI, Akiyama I, Tonaki D, Hirose H, Takahashi S, Takahashi Y (2007) Amino acid limitation induces expression of ATF5 mRNA at the post-transcriptional level. Life Sci 80:879–885
49. Zhou D, Palam LR, Jiang L, Narasimhan J, Staschke KA, Wek RC (2008) Phosphorylation of eIF2 directs ATF5 translational control in response to diverse stress conditions. J Biol Chem 283:7064–7073

Fig. Legends

Fig. 1

As in rodents, ATF5 is expressed by adult human neurons and it accumulates in the characteristic HD nuclear inclusions in both species. **a.** Immunohistochemistry with ATF5 antibody in cortex (Cx; top) and striatum (St; bottom) of 3.5 month-age R6/1 and wild-type (WT) mice. Black arrowheads in R6/1 panels (left) show ATF5 accumulation into inclusion bodies in Cx and St. **b.** Immunohistochemistry with ATF5 antibody in Cx (top) and St (bottom) postmortem tissue of HD patients and control subjects. Black arrowheads in HD panels (*left*) show ATF5 accumulation into inclusion bodies in Cx and St. **c.** ATF5 immunohistochemistry and nuclear counterstaining in Cx post-mortem tissue of HD patients. *Black arrowheads* indicate that ATF5 can be found not only in nuclear inclusions (*both panels*) but also in cytoplasmic inclusions in the soma (*left panel*), in neuritic inclusions (*right panel*), and in neuropil inclusions (*right panel*). *White arrow-heads* point to nucleoli to show that they are not coincident with the nuclear inclusions

Fig. 2:

Fig. 2 ATF5-positive neuronal nuclear inclusions colocalize with the characteristic polyQ-containing inclusions in HD mice and human tissue. Double immunofluorescence with ATF5 (green) and HTT (EM48, red) antibodies in St of 3.5 month-age R6/1 mice (**a**) and in Cx of HD patients (**b**). White arrowheads show ATF5 positive intra-nuclear inclusion bodies. *Dashed lines* delimit the regions taken for magnification and colocalization analysis. Orthogonal images (*right panels*) show colocalization of ATF5 and mHTT immunofluorescence projected in *YZ* and *XZ* axis. Nuclei were counterstained with DAPI (*blue*)

Fig. 3:

Decreased ATF5 levels in striatum and cortex of HD mouse model and human tissue. **a.** Representative western blots of ATF5 protein levels in Cx and St of 3.5 month-age R6/1 mice (*n* = 9) and WT mice (*n* = 9). **b.** Representative western blots of ATF5 protein levels in Cx and St of HD patients (*n* = 9) compared to their respective controls (*n* = 9). ATF5 is normalized by β-ACTIN in all samples and also by TUBB3 in human samples. Histograms show quantification of ATF5 protein abundance with respect to control (Student's *t* test; **p* < 0.05, ***p* < 0.01, ****p* < 0.001). Data represent mean ± SEM

Fig. 4:

Decreased levels of the antiapoptotic protein MCL1 in striatum and cortex of HD mouse model and human tissue. **a.** Representative western blots of MCL1 protein levels in Cx and St of 3.5 month-age R6/1 mice (*n* = 7) and WT mice (*n* = 7). **b.** Representative western blots of MCL1 protein levels in Cx and St of HD patients (*n* = 7) compared to their respective controls (*n* = 7). Histograms show quantification of MCL1 protein abundance with respect to control (Student's *t* test; **p* < 0.05, ***p* < 0.01, ****p* < 0.001). Data represent mean ± SEM

Fig. 5:

Deleterious effect of ATF5 deficiency in a *C. elegans* model of polyQ toxicity. **a.** Brightfield and fluorescence images of *wt*, *atf-5(tm4397)*, *Q40::yfp* and *Q40::yfp; atf-5(tm4397)* worms. **b.** Quantification of the number of Q40::YFP aggregates in *Q40::yfp* and *Q40::yfp; atf-5(tm4397)* animals (*n* = 20; Student's *t* test; **p* < 0.05). **c.** Quantification of the number of body bends/min in *wt*, *atf-5(tm4397)*, *Q40::yfp* and *Q40::yfp; atf-5(tm4397)* worms (*n* = 20). Analysis of variance

(ANOVA), followed by minimum significant difference or Games–Howell, *$p < 0.05$, ***$p < 0.001$. Data represent mean ± SEM

Fig. 6:

ATF5 protects against polyQ-induced apoptosis in a cell model of HD. **a.** Representative western blot of ATF5 and MCL1 protein levels upon pcDNA-MYC-mATF5 (ATF5) transfection of N2a neuroblastoma cells. The histogram shows the abundance of MCL1 protein in transfected cells with respect to the control (Mock) (n = 6; Student's t test). **b.** Immunofluorescence analysis of ATF5 pattern in N2a cells transfected with toxic PolyQ94-CFP only (PolyQ94) or in combination with ATF5 (PolyQ94 and ATF5) shows accumulation of ATF5 within polyQ-containing inclusions (*yellow arrow-heads*) in both paradigms and that ATF5 overexpression results also in increased diffuse ATF5 staining in PolyQ94 and ATF5. **c.** Apoptosis induction analysis by immunofluorescence of cleaved caspase-3 (c-c3) and nuclear morphology (DAPI) in N2a cells transfected with either PolyQ16, PolyQ94 or PolyQ94 and ATF5. **d.** Quantification of apoptotic cell death in N2a cells transfected with either PolyQ16, PolyQ94 or PolyQ94 and ATF5 with respect to the total number of cells counted (n = 300). Analysis of variance (ANOVA), followed by minimum significant difference or Games–Howell. **e.** Western blot analysis of MCL1 protein levels upon p3XFlag-CMV10-Flag-mMcl-1 (MCL1) transfection of N2a cells. The histogram shows the abundance of MCL1 protein in transfected cells with respect to the control (Mock) (n = 2; Student's t test). **f.** Apoptosis induction analysis by immunofluorescence of cleaved caspase-3 (c-c3) and nuclear morphology (DAPI) in N2a cells transfected with either PolyQ16, PolyQ94 or PolyQ94 and MCL1. **g.** Quantification of apoptotic cell death in N2a cells transfected with either PolyQ16, PolyQ94 or PolyQ94 and MCL1 with respect to the total number of cells counted (n = 700). Analysis of variance (ANOVA), followed by minimum significant difference or Games–Howell, *$p < 0.05$, ***$p < 0.001$. Data represent mean ± SEM

Fig. 1

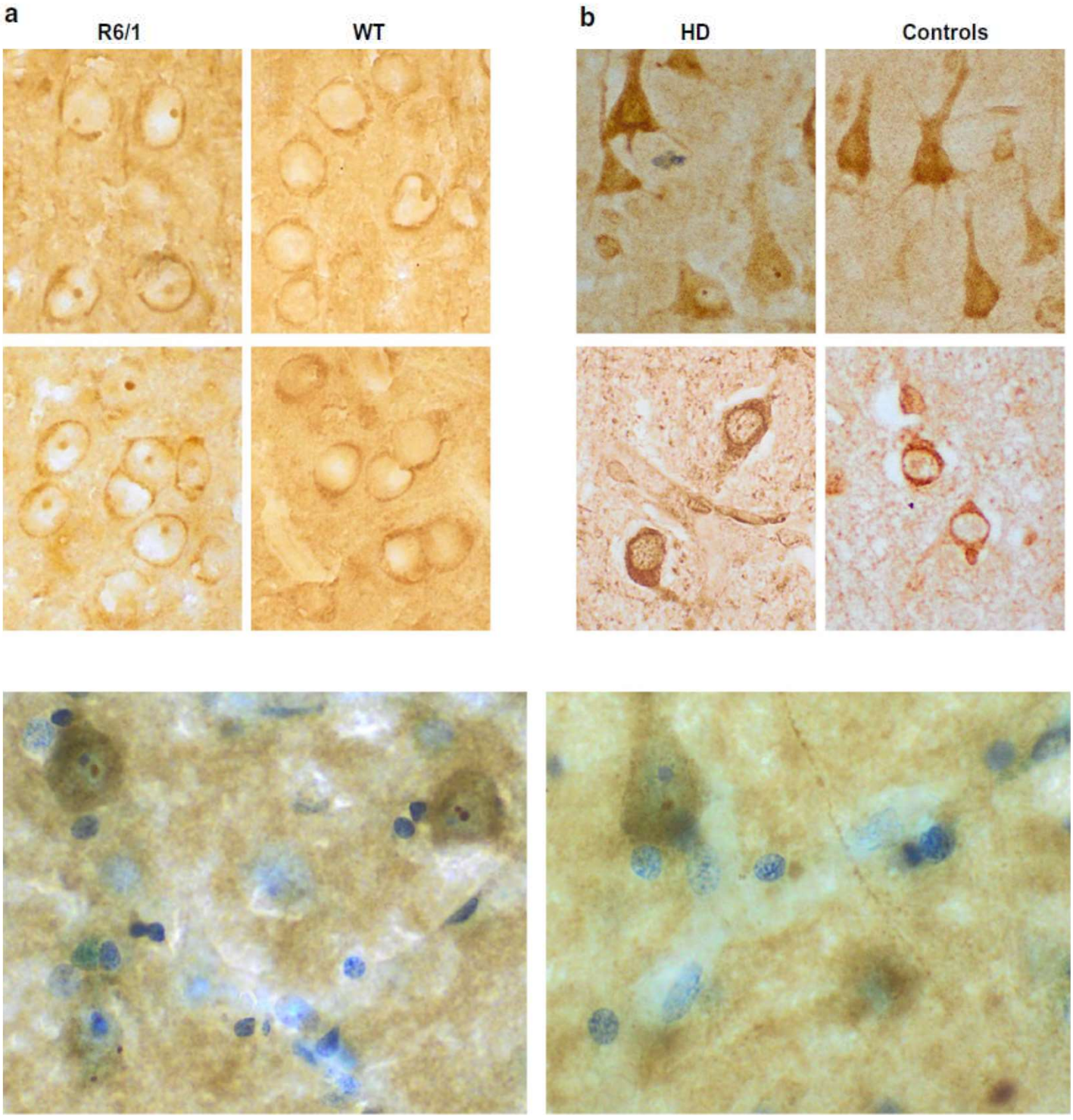

Fig. 2

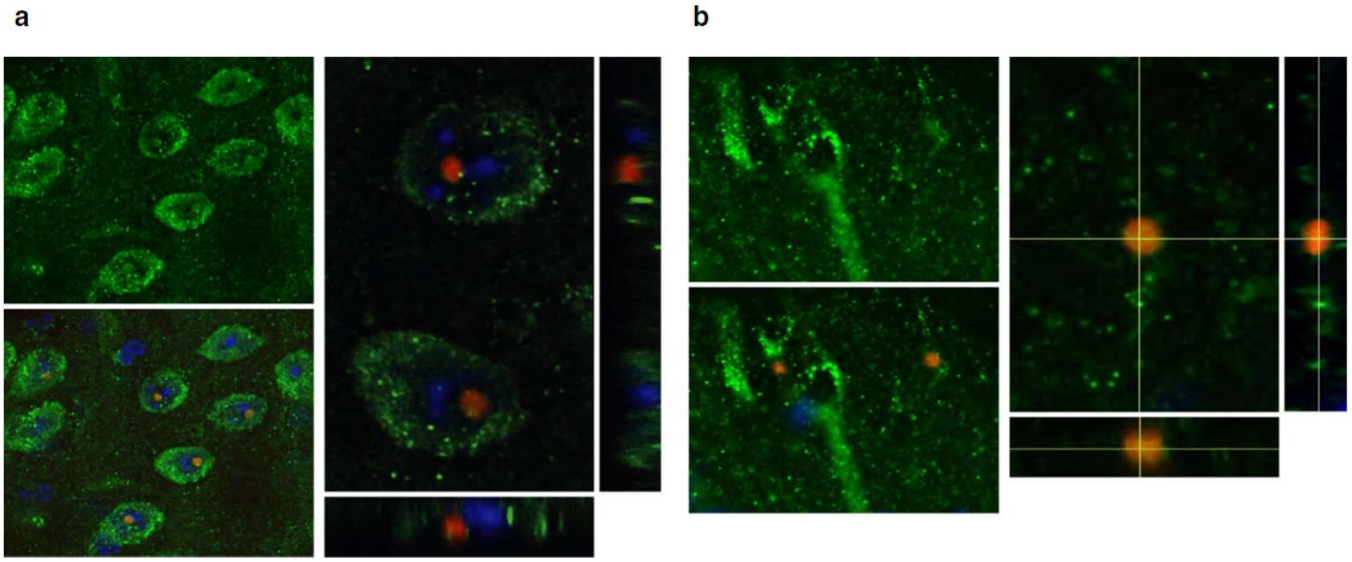

Fig. 3

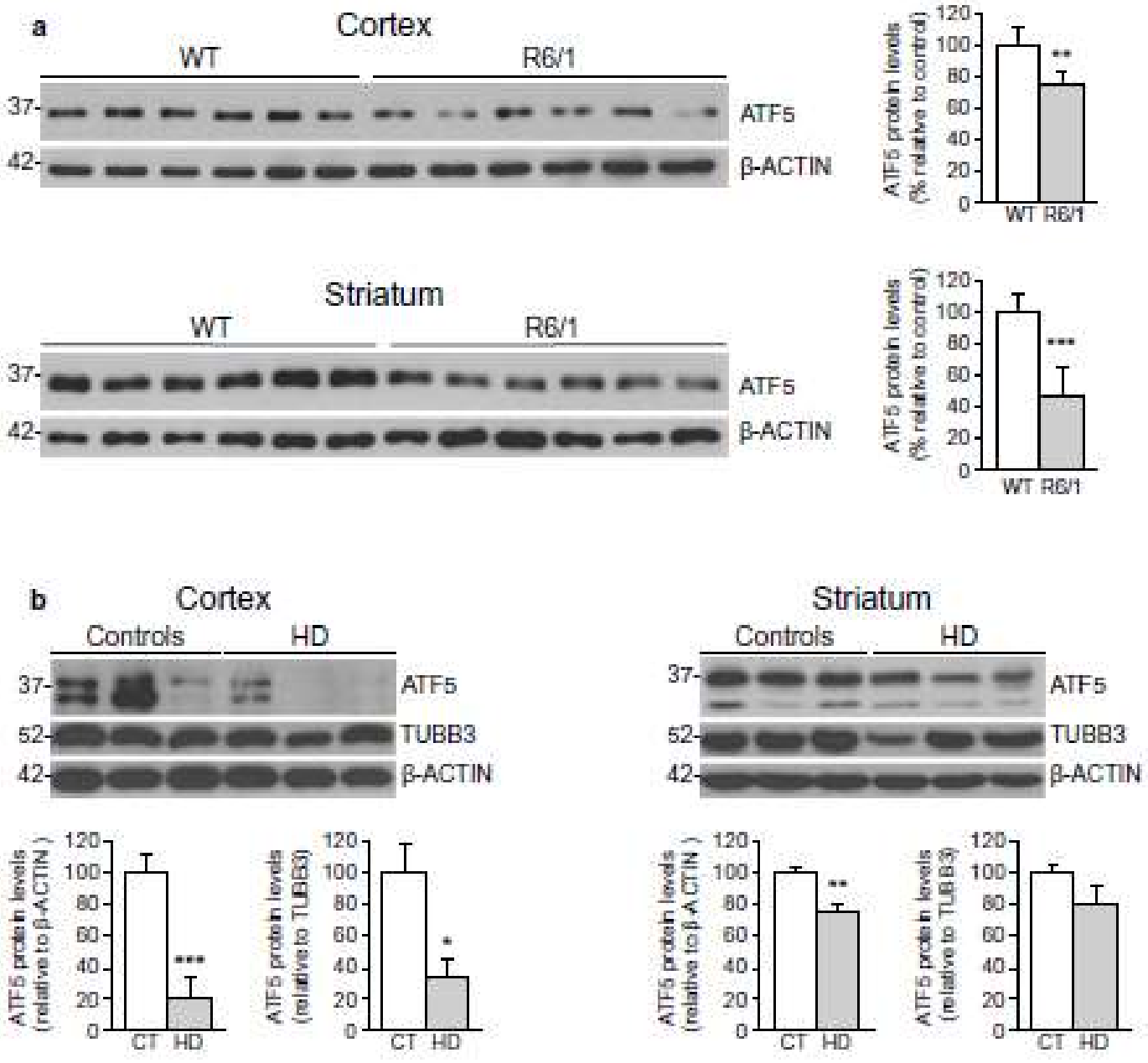
a
Cortex
WT
R6/1
37-
42-
ATF5
β-ACTIN
ATF5 protein levels (% relative to control)
**
WT R6/1
Striatum
***
b
Controls
HD
52-
TUBB3
ATF5 protein levels (relative to β-ACTIN)
ATF5 protein levels (relative to TUBB3)
*
CT HD

Fig. 4

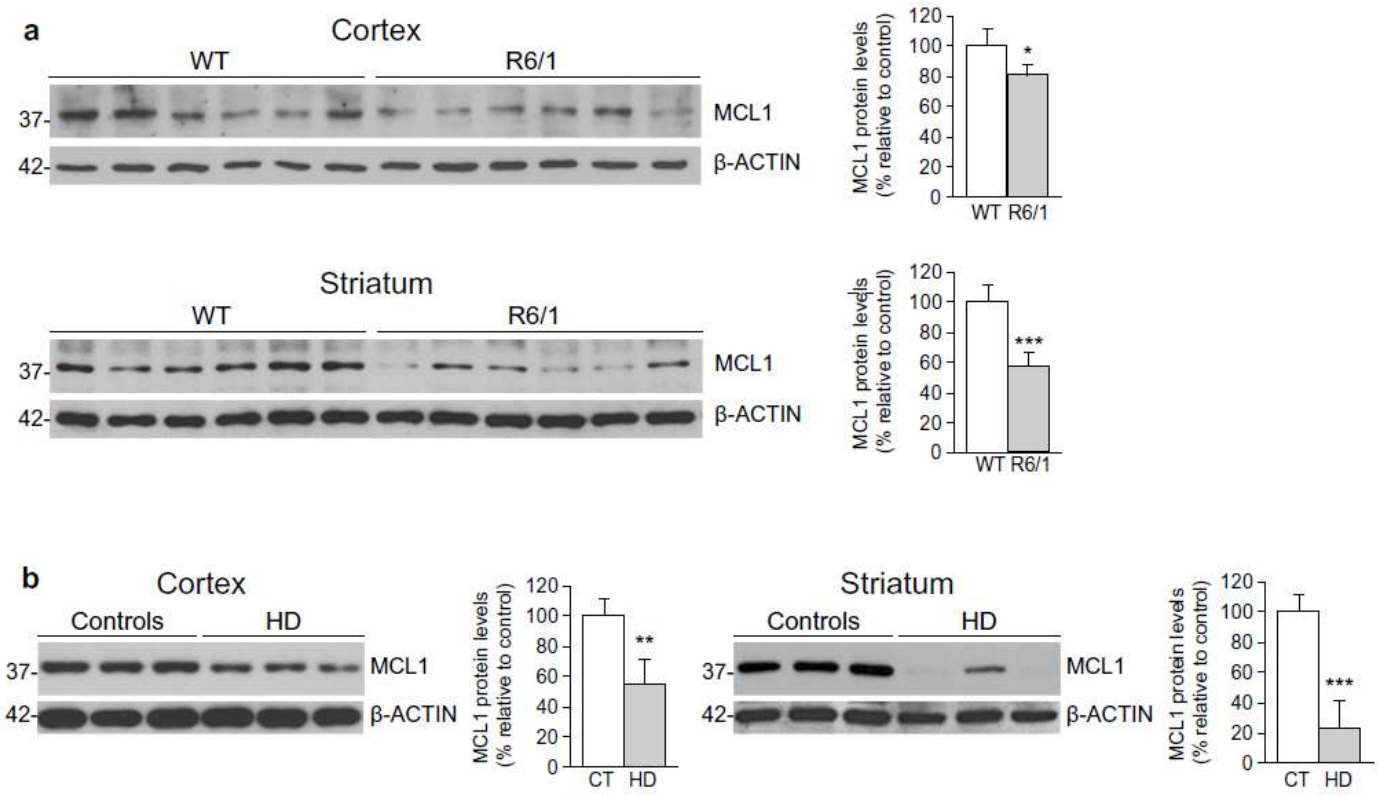
a
Cortex
WT
R6/1
37-
42-
MCL1
β-ACTIN
MCL1 protein levels (% relative to control)
120
100
80
60
40
20
0
*
WT R6/1
Striatum
WT
R6/1
37-
42-
MCL1
β-ACTIN
MCL1 protein levels (% relative to control)
120
100
80
60
40
20
0
***
WT R6/1
b
Cortex
Controls
HD
37-
42-
MCL1
β-ACTIN
MCL1 protein levels (% relative to control)
120
100
80
60
40
20
0
**
CT HD
Striatum
Controls
HD
37-
42-
MCL1
β-ACTIN
MCL1 protein levels (% relative to control)
120
100
80
60
40
20
0
***
CT HD

Fig. 5

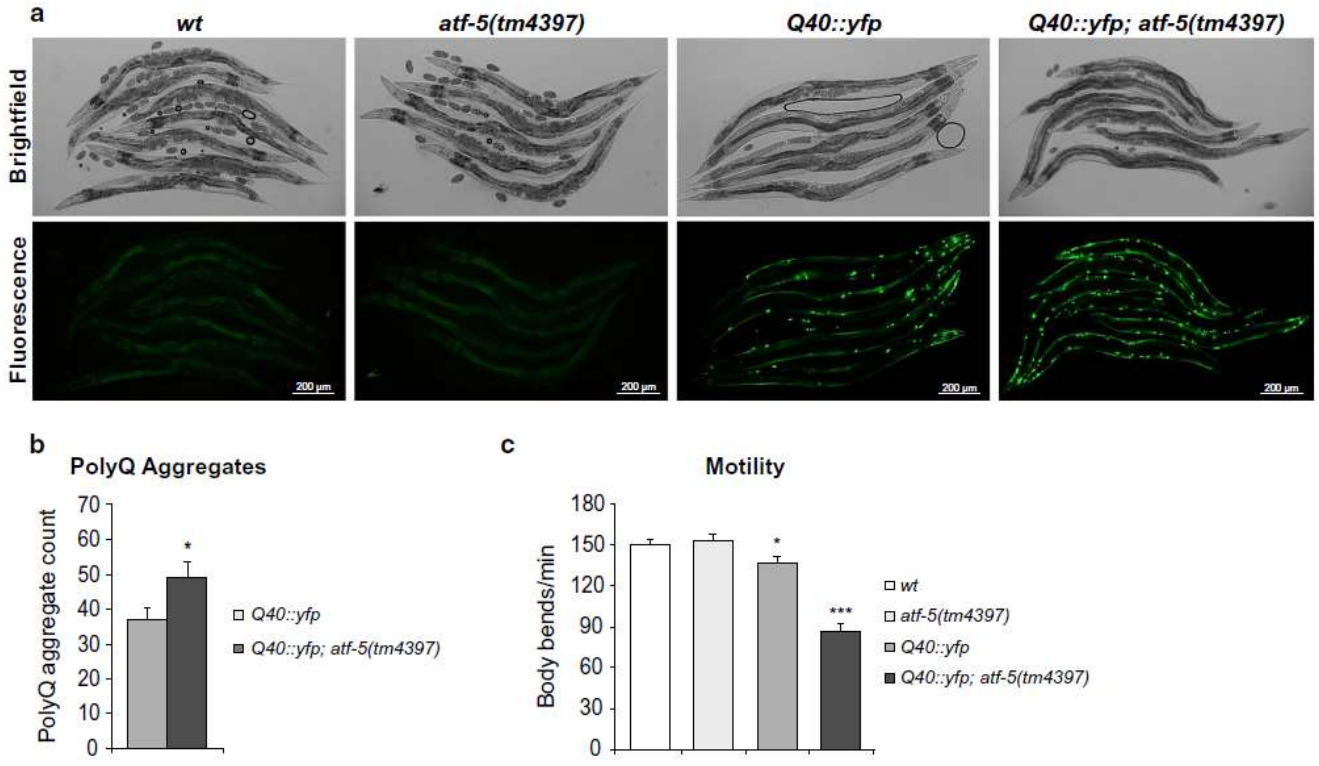
a
wt
atf-5(tm4397)
Q40::yfp
Q40::yfp; atf-5(tm4397)
Brightfield
Fluorescence
200 µm
b
PolyQ Aggregates
PolyQ aggregate count
70
60
50
40
30
20
10
0
*
Q40::yfp
Q40::yfp; atf-5(tm4397)
c
Motility
Body bends/min
180
150
120
90
60
30
0
*
***
wt
atf-5(tm4397)
Q40::yfp
Q40::yfp; atf-5(tm4397)

Fig. 6

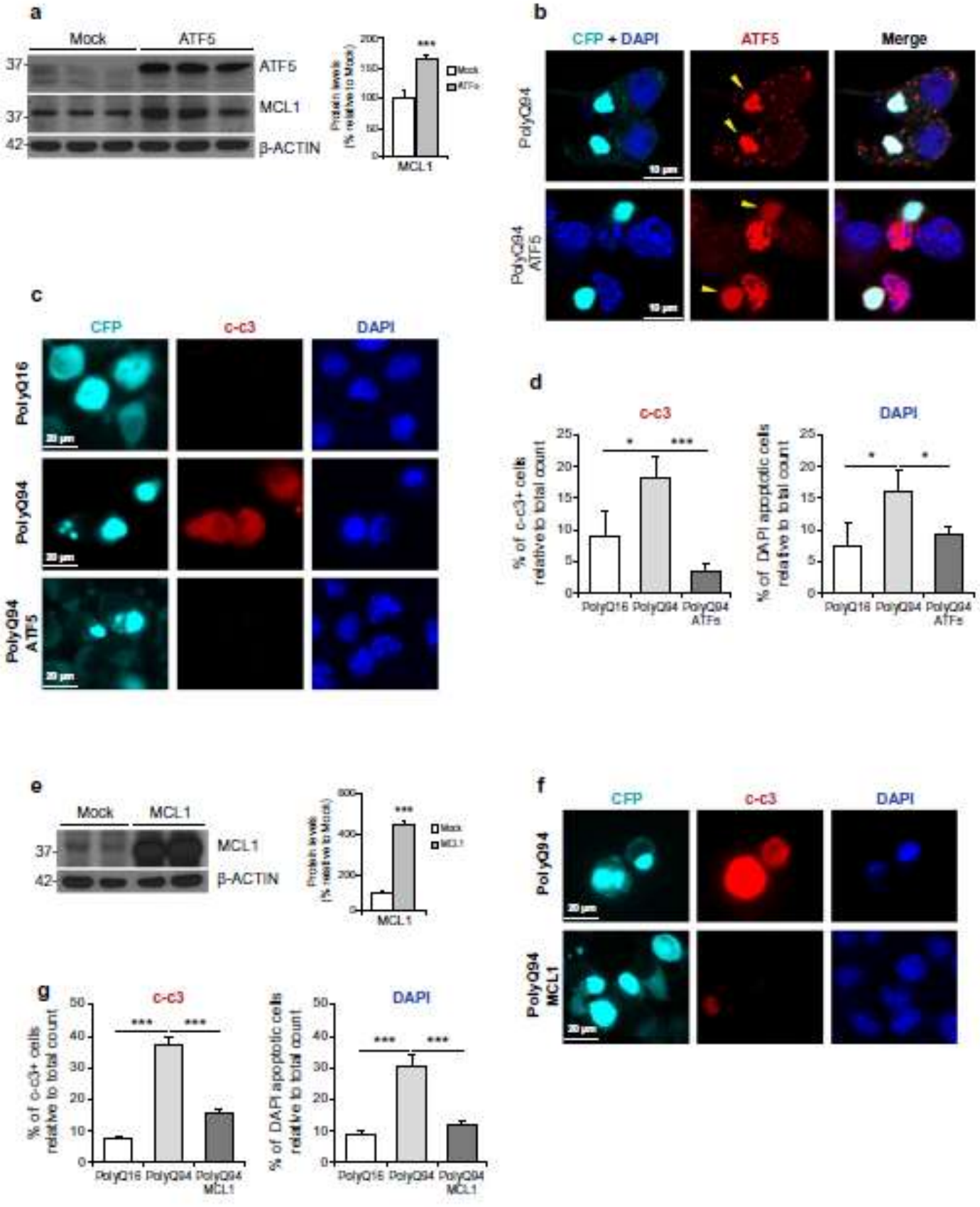
a
Mock
ATF5
37
ATF5
MCL1
37
42
β-ACTIN
MCL1
b
CFP + DAPI
ATF5
Merge
PolyQ94
PolyQ94 ATF5
c
CFP
c-c3
DAPI
PolyQ16
PolyQ94
PolyQ94 ATF5
d
c-c3
DAPI
% of c-c3+ cells relative to total count
% of DAPI apoptotic cells relative to total count
PolyQ16
PolyQ94
PolyQ94 ATFs
e
Mock
MCL1
37
MCL1
42
β-ACTIN
MCL1
f
CFP
c-c3
DAPI
PolyQ94
PolyQ94 MCL1
g
c-c3
DAPI
% of c-c3+ cells relative to total count
% of DAPI apoptotic cells relative to total count
PolyQ16
PolyQ94
PolyQ94 MCL1